QUANTIFYING THE PARTICLE SIZE OF INTERTIDAL SEDIMENTS WITH SATELLITE REMOTE SENSING IN THE VISIBLE LIGHT, THERMAL INFRARED AND MICROWAVE SPECTRAL DOMAIN

D. van der Wal *, P.M.J. Herman

Centre for Estuarine and Marine Ecology, Netherlands Institute of Ecology (NIOO-KNAW),
P.O. Box 140, 4400 AC Yerseke, The Netherlands

KEY WORDS: SAR, VNIR, TIR, sediment grain-size, mapping, regression modelling, synergy

ABSTRACT:

Information on sediment grain-size of intertidal areas is required for coastal management, e.g. for habitat and ecotope mapping and dredging studies. This study aims to derive such information from visible and near-infrared (VNIR), shortwave-infrared (SWIR), and thermal infrared (TIR) remote sensing as well as Synthetic Aperture Radar (SAR) using satellite imagery. Surface reflectance in the VNIR and SWIR was derived from a Landsat ETM+ L1G image, surface emissivity in the TIR was obtained from a Terrra ASTER L2_05 image, and the backscattering coefficient was estimated from an ERS-2 SAR PRI image. Corroborative data of the median grain-size of the sediment was obtained during field campaigns on an intertidal flat in the Westerschelde (southwest Netherlands). Algorithms have been developed using regression modelling; they were based on the separate remote sensing sources, as well as on synergy of information derived from the different sensors. The algorithms were applied to the satellite imagery to generate maps of the particle size of intertidal sediments. In all spectral domains, significant results have been achieved. A combination of VNIR, TIR and SAR was found to yield best results for mapping the particle size of intertidal sediments.

1. INTRODUCTION

Estuarine intertidal flats, shaped by a combination of coastal and fluvial processes, can exhibit complex sediment characteristics. There is a great need for information on the sediment characteristics of such intertidal flats to assist coastal management, for instance for habitat mapping, pollution and nutrient studies, and ecological impact assessments, including the ecological impact of dredging and dredge spoil dumping. Remote sensing can provide high resolution, synoptic information on the sediment characteristics of intertidal flats.

Optical remote sensing has been used in various studies to map the grain-size of intertidal sediments using satellite sensors, employing (un)supervised classification techniques, spectral mixture modelling and regression modelling, with corroborative information of grain-size from field samples (e.g., Bartholdy & Folving, 1986; Yates et al., 1993; Van der Wal & Herman, 2006). Recently, hyperspectral airborne sensors have been used, typically operating in the visible and near-infrared (VNIR) and short-wave infrared (SWIR) spectral domain, (e.g. Rainey et al., 2003; Smith et al., 2004). In all studies, the positive correlation of surface reflectance and grain-size was not due to a direct relationship, but was based on a negative relationship between sediment grain-size and moisture content, and a negative relationship between soil moisture content and surface reflectance in the VNIR and SWIR (Baumgardner et al., 1985).

Melsheimer et al. (1999) and Van der Wal et al. (2005) applied microwave (SAR) remote sensing to quantify the sediment grain-size of intertidal flats. In this case, the correlation between sediment grain-size and C-band backscattering is due to the fact that C-band backscattering is especially sensitive to, and positively related to surface roughness, and that sediment grain-size is also positively correlated with surface roughness on an intertidal flat, as surface ripples best form in coarser sediment (Van der Wal et al., 2005). Interstitial moisture content of intertidal sediments was found to be too high to significantly influence the C-band backscattering signal. This allowed successful mapping of sediment grain-size from SAR (Van der Wal et al., 2005).

So far, thermal infrared (TIR) has received little attention for mapping sediment grain-size on intertidal flats. Salisbury & D'Aria (1992b) demonstrated that soils can be characterised based on emissivity spectra from TIR imagery obtained from the Terra (EOS) ASTER satellite. Quartz displays strong fundamental molecular vibration bands or Reststrahlen bands, resulting in broad reflectance peaks (and, following Kirchoff's Law, emittance troughs), including the reflectance doublet between 8 and 9.5 μm (Salisbury & D'Aria, 1992a). For sediments dominated by quartz, the magnitude of the Reststrahlen bands was found to correlate with particle size (Salisbury & Eastes, 1985; Salisbury & D'Aria, 1992b). However, organic matter, moisture conditions and vegetation can be complicating factors.

The objective of this study is to explore, compare and combine the use of optical, thermal infrared and microwave remote sensing to map the grain-size of intertidal sediments. A regression-based approach is adopted. The focus is on an intertidal flat in the Westerschelde (southwest Netherlands).

2. STUDY SITE

The Westerschelde (Figure 1) is a tide-dominated estuary, with a semi-diurnal tide. The estuary is characterised by a complex network of flood and ebb channels surrounding intertidal flats. The study focuses on the Molenplaat, an unvegetated tidal flat, experiencing a mean tidal range of ca 4.5m. The flat has sandy to muddy sediment, which is mainly composed of quartz sand,

* Corresponding author. d.vanderwal@nioo.knaw.nl

with a substantial amount of illite, and to a lesser extent kaolinite and smectite in the clay fraction.

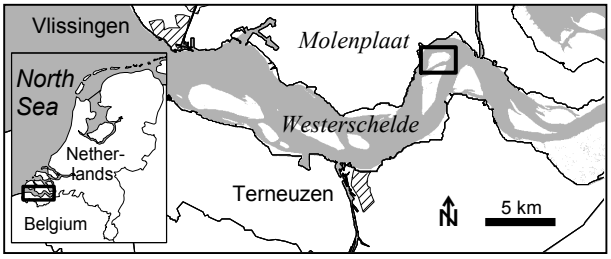

Figure 1. Molenplaat (shown in black rectangle) in the Westerschelde, southwest Netherlands.

3. METHODS

3.1 Processing of satellite imagery

3.1.1 Surface reflectance from a Landsat 7 ETM+ image

A Landsat 7 ETM+ L1G image (Table 1), acquired during low, outgoing tide, was imported into Erdas Imagine Professional for preprocessing. The image was acquired in SLC-off mode, resulting in an absence of data for certain areas (strips). Digital Numbers in the visible and infrared bands (TM1 to TM5 and TM7) were converted to surface reflectance values taking into account the gains/bias information of the scene, solar angle, solar spectral irradiance and sun-earth distance. The images were rectified and transformed to the Dutch National Grid using ground control points, applying a nearest neighbour resampling technique, while retaining the original pixel size of 30 m. Reflectance values were then averaged, using a moving window of 3 by 3 pixels (corresponding to 90 m in the field). An Empirical Line Calibration was carried out to correct for atmospheric effects, using a corrected reference Landsat 7 ETM+ image; this procedure is described in detail by Van der Wal & Herman (2006). Reflectance values (expressed as a value from 0 to 1) for the blue band (R_{TM1}), green band (R_{TM2}), red band (R_{TM3}), near-infrared (NIR) band (R_{TM4}), and mid-infrared (SWIR) bands (R_{TM5} and R_{TM7}) were used for further analysis.

3.1.2 Surface emissivity from a Terra ASTER image

Surface emissivity was derived from a Terra ASTER L2 (AST_05) product (Table 1), that was atmospherically corrected by NASA. The image was acquired during low, incoming tide. Only the western part of the Molenplaat was covered by the image. The image contains surface emissivity data at 90 m spatial resolution, derived from five thermal infrared (TIR) bands (Table 2). They are derived using a temperature/emissivity separation algorithm from ASTER L2 surface radiance data. Surface emissivity is defined as the ratio of energy emitted from the surface to the energy emitted from a true blackbody at an equivalent temperature, for a specific wavelength, expressed as a value from 0 to 1. The emissivity images were rectified and transformed to the Dutch National Grid projection. Apart from the emissivity values in all five bands, a band ratio was derived from the emissivity in ASTER band 10 (E_{AST10}) and band 14 (E_{AST14}), i.e. $E_{AST10/AST14}$. This index was found to be valuable for identifying grain-size by Salisbury & D'Aria (1992b).

3.1.3 Backscattering from an ERS-2 SAR image

An ERS-2 SAR PRI image (Table 1) was acquired during low tide. This is a multi-look (noise-reduced), ground range, system-corrected digital image of C-band microwave data. The data were calibrated following Laur et al. (2002) and Van der Wal et al. (2005). Brightness values β^0 were converted to estimates of the backscattering coefficient σ^0, assuming flat terrain. Differences in incident angle occurring across a swath were included in this conversion. The radiometric resolution was enhanced by applying a 9 by 9 moving average window (corresponding to ca 112 by 112 m in the field). The images were rectified and transformed to the Dutch National Grid, applying a cubic convolution interpolation technique, while retaining the pixel size of 12.5 by 12.5 m. Finally, backscattering coefficients were expressed in decibels.

Satellite/ instrument	Date/ time (UTM)	Track (path)	Frame (row)	Water level (m)
Landsat 7 ETM+	18 Sep 10:28	198	24	-0.90
Terra ASTER	16 Jul 10:56	200	24	-1.40
ERS-2 SAR	29 Sep 10:40	194	2565	-1.88

Table 1. Specification of the satellite imagery acquired in 2003. Actual water level (relative to Dutch ordnance datum NAP, which is about mean sea level) during overpass were obtained from Rijkswaterstaat for nearby station Hansweert.

3.2 Field campaigns and laboratory analysis

Ground truthing took place on 29 September and 1-2 October 2003, matching the selected images. Samples were collected during low tide on the Molenplaat, along a southwest to northeast oriented transect as well as on random locations. The sampling sites were located using a GPS with 4 m accuracy. At the stations, 20 cm^3 of sediment was taken from the upper 3 cm of the sediment. The samples were freeze-dried. Median grain-size of the sediment (d_{50}, in mm) was determined from these samples using a Malvern particle sizer. The sampling sites located above -1.0 m NAP were selected for further analysis.

3.3 Statistical analysis and mapping

The field data were joined in a Geographical Information System (ArcGIS) to values for surface reflectance, surface emissivity and estimates of the backscattering coefficients, derived from the three matching images. Statistical data analysis was carried out using the software package Statistica. All tests were performed applying a significance level of 0.05. Significant relationships between variables were assessed by calculating the product moment correlation coefficient (with a value of -1.00 representing a perfect negative correlation and a value of 1.00 representing a perfect positive correlation). (Multiple) least-squares regression analysis was undertaken on the data for mapping the median grain-size as a function of the measures derived from remote sensing. The coefficient of determination (R^2), number of observations (n), probability (p) and standard error of estimate ($s.e.$) of the regressions are given in the text. The regression equations were applied to the image data to generate maps of median grain-size of the sediment.

4. RESULTS

4.1 Particle size and remote sensing measures

In Table 2, product moment coefficients are presented for the correlation between sediment grain-size and the measures from VNIR/SWIR, TIR and microwave (SAR) remote sensing. In the visible (VIS) and near-infrared (NIR), best correlations with sediment grain-size were found for surface reflectance in the green R_{TM2} (r=0.81) and in the near-infrared R_{TM4} (r=0.73). Correlations in the SWIR were significant, but very weak. Negative correlations were found for all TIR bands, except for band 14 (E_{AST14}). Figure 2 shows the spectral curves for five grain-size classes, with lower emissivity, as well as stronger spectral contrast for the larger grain-sizes. From the graph, it can be deduced that the index $E_{AST12/AST14}$, rather than $E_{AST10/AST14}$ would be most appropriate to characterise grain-size on intertidal flats. Indeed, Table 2 confirms that the index $E_{AST10/AST14}$ only shows a weak correlation with median grain-size, and that $E_{AST12/AST14}$ shows a stronger correlation. Best correlations were found between median grain-size and E_{AST11} and E_{AST12} (r=-0.59). There was also a good correlation between sediment grain-size and C-band backscattering σ^0 (r=0.70). Figure 3 gives scatter plots showing the relation between median grain-size and three parameters that gave strong correlations, i.e. reflectance in the green R_{TM2}, surface emissivity E_{AST12} and the C-band backscattering coefficient σ^0.

Spectral region	Wavelength (μm)	Measures	r	n	p
VIS	0.450-0.515	R_{TM1}	0.67	110	0.000
	0.525-0.602	R_{TM2}	0.81	110	0.000
	0.630-0.690	R_{TM3}	0.62	110	0.000
NIR	0.750-0.900	R_{TM4}	0.73	110	0.000
SWIR	1.550-1.750	R_{TM5}	0.21	110	0.024
	2.090-2.350	R_{TM7}	0.28	110	0.003
TIR	8.125-8.475	E_{AST10}	-0.52	79	0.000
	8.475-8.825	E_{AST11}	-0.59	79	0.000
	8.925-9.275	E_{AST12}	-0.59	79	0.000
	10.25-10.95	E_{AST13}	-0.47	79	0.000
	10.95-11.65	E_{AST14}	-0.09	79	0.438
	-	$E_{AST10/AST14}$	-0.50	79	0.000
	-	$E_{AST12/AST14}$	-0.58	79	0.000
Microwave	5.66 cm	σ^0	0.70	126	0.000

Table 2. Product moment correlation coefficients r, number of observations n and significance p for correlations between the median grain-size and the indices derived from remote sensing.

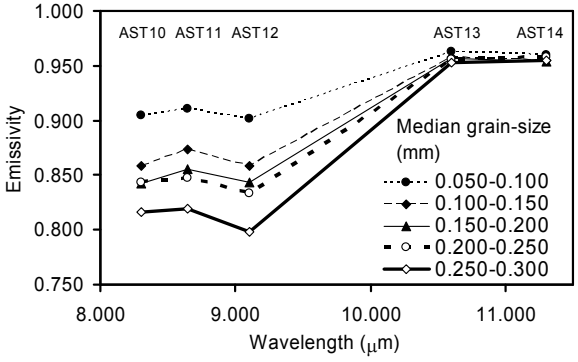

Figure 2. Emissivity derived from the five ASTER TIR bands AST10-14, averaged for five grain-size classes.

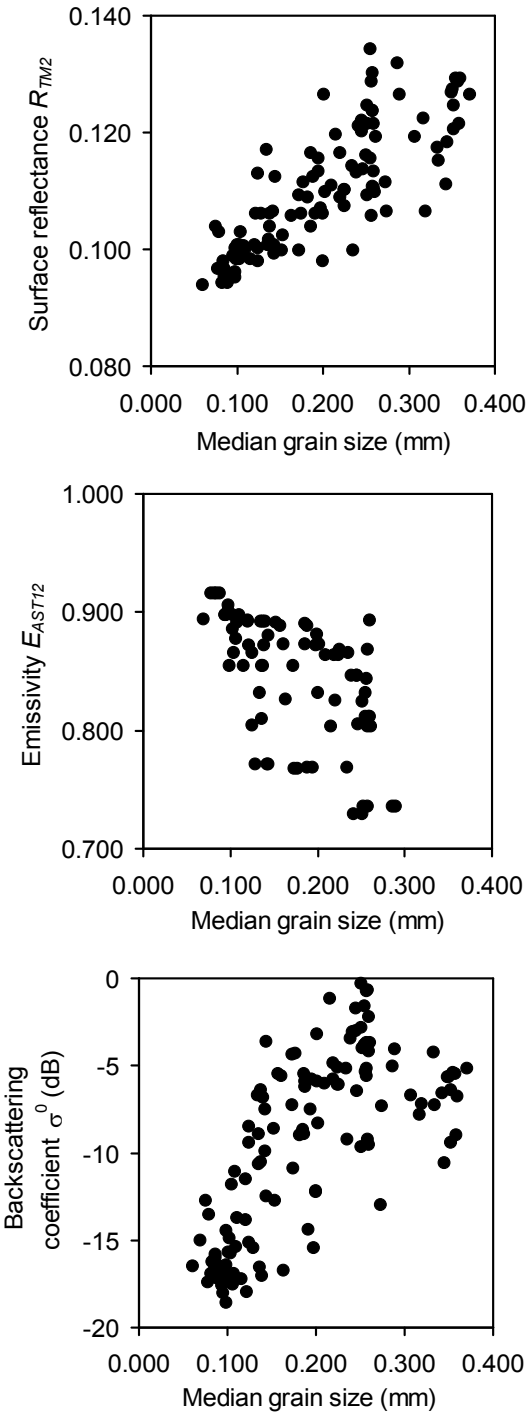

Figure 3. Scatter plots of median grain-size versus remote sensing measures.

4.2 Mapping particle size

Three regression equations were established based on the indices from remote sensing and matching field data, to assess the median grain-size (in mm) of intertidal sediments:

$$d_{50} = 6.576\ R_{TM2} - 0.524 \quad (1)$$

with R^2=0.65, *s.e.* =0.0503, n=110, p=0.000,

$$d_{50} = -0.705\ E_{AST12} + 0.771 \quad (2)$$

with R^2=0.35, *s.e.*=0.0506, n=79, p=0.000, and

$$d_{50} = 0.0114\ \sigma^0 + 0.300 \quad (3)$$

with R^2=0.48, *s.e.* =0.0607, n=126, p=0.000.

Of these regression equations, most variation was explained by $R_{TM2,}$ whereas the standard error was smallest for R_{TM2} and E_{AST12}. When combining the measures from Table 2 in a backward multiple linear regression, eliminating redundant variables, the following regression equation was obtained:

$$d_{50} = 3.475\ R_{TM2} - 0.772\ E_{AST10} + 0.868\ E_{AST12} + 0.00615\ \sigma^0 - 0.2211 \quad (4)$$

with R^2=0.79, *s.e.* =0.0295, n=64, p=0.000.

The combination of measures was found to give best performance, both regarding the amount of variation explained and the standard error. Figure 4 shows a comparison of median grain-size predicted from the remote sensing measures (eq. 4) and observed from field samples; a good 1:1 relationship between observed and predicted grain-size is achieved.

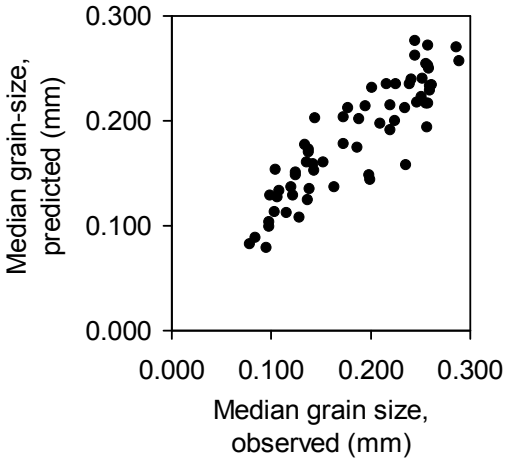

Figure 4. Scatter plot of median grain-size predicted with eq. 4 versus observed values from field samples.

The regression equations were applied to the three satellite imagery to obtain maps of the sediment grain-size for the Molenplaat (Figure 5). In general, comparable results were found, with a muddy and sandy belt alternating in the west and a more muddy area in the central part of the Molenplaat. Larger particle sizes (d_{50}>0.300 mm) were found in the eastern part of the Molenplaat, but both the map derived from R_{TM2} and the map derived from σ^0 underestimated particle grain-size in this area in places. Unfortunately, no TIR data were available for this area.

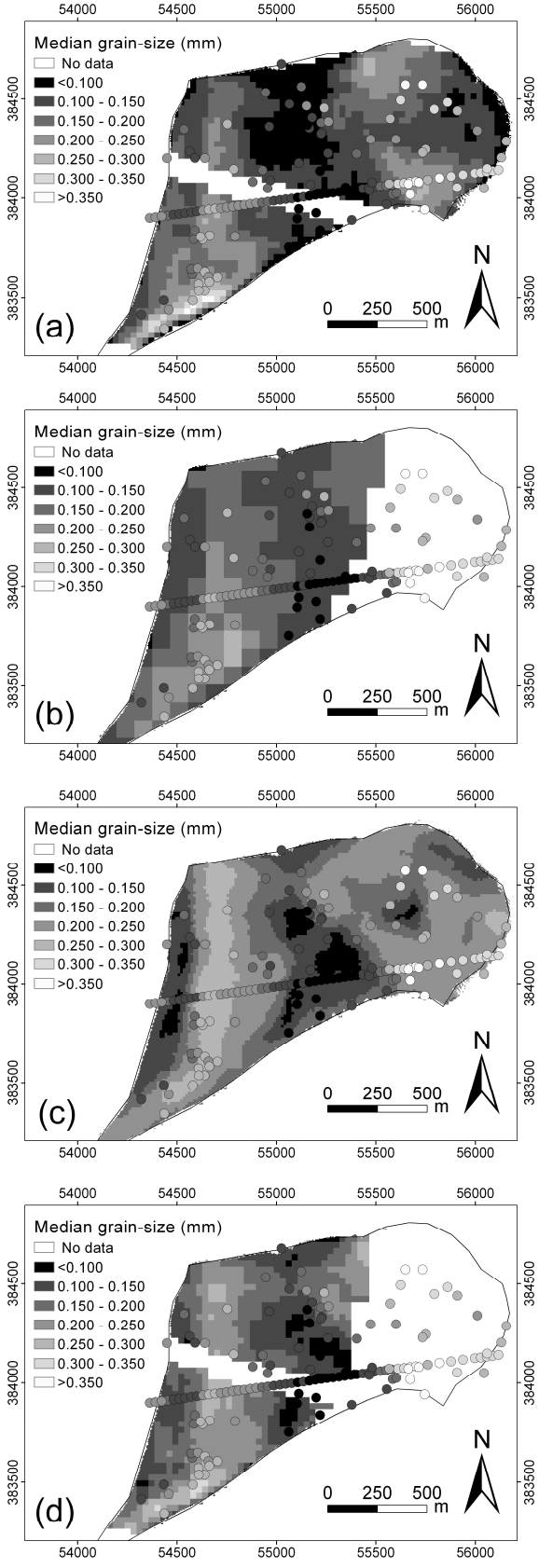

Figure 5. Maps of median grain-size applying regression equations based on remote sensing measures, i.e. (a) $R_{TM2,}$ see eq. 1, (b) E_{AST12}, see eq. 2, (c) σ^0, see eq. 3, and (d) a combination , see eq. 4. Dots represent median grain-size from field samples. Outline is the -1.0 m NAP contour.

5. DISCUSSION AND CONCLUSIONS

This paper shows that sediment grain-size of intertidal flats can be mapped using information from remote sensing in a number of spectral domains. Best results were obtained for mapping median grain-size using information in the green part of the visible light, followed by information from the microwave domain, i.e., the C-band backscattering coefficient.

A weak, but significant relationship was found between median grain-size and emissivity in the thermal infrared, in particular for E_{AST11} and E_{AST12}. Salisbury & D'Aria (1992b) demonstrated a similar dependence of emissivity in the thermal infrared spectral domain on particle size: sediment with coarser particles was found to show a stronger spectral contrast in the Reststrahlen bands. However, other constituents of the sediment also influence the emissivity spectrum. (Sea)water has a high emissivity (ca 0.94-0.99) across the thermal infrared region. Water is strongly absorbing in the region of the quartz Reststrahlen bands, resulting in a sharp decrease in spectral contrast, as well as an increase in emissivity with increasing soil moisture content (Salisbury & D'Aria, 1992b). Organic matter is also highly absorbing in the TIR region, reducing the apparent spectral contrast of the quartz Reststrahlen bands (Salisbury & D'Aria, 1992b). Vegetation can also mask the sediment spectrum; on an intertidal flat, a similar effect can be expected from the presence of microphytobenthos. Soil moisture, organic matter and to a lesser extent chlorophyll-*a* (as a proxy for microphytobenthos cover) are all inversely correlated with particle size of intertidal sediments (Yates et al., 1993; Van der Wal et al., 2005). This enhances the negative correlation between particle size and emissivity in the thermal infrared. Thus, moist sandy sediment has a lower emissivity than very moist muddy sediment.

In our study, a combination of information in the visible light, thermal infrared and microwave remote sensing yields the best prediction of particle size of intertidal sediments on the Molenplaat. This demonstrates the benefits of a multi-sensor approach for mapping intertidal sediments.

REFERENCES

Bartholdy, J., & Folving, S., 1986. Sediment classification and surface type mapping in the Danish Wadden Sea by remote sensing. *Netherlands Journal of Sea Research*, 20: 337-345.

Baumgardner, M.F., Silva, L.F., Biehl, L.L. & Stoner, E.R., 1985. Reflectance properties of soils. *Advances in Agronomy* 38: 1-44.

Laur, H., Bally, P., Meadows, P., Sanchez, J., Schaettler, B., Lopinto, E., & Esteban, D., 2002. ERS SAR Calibration. Derivation of the Backscattering Coefficient σ^0 in ESA ERS SAR PRI Products. Document ES-TN-RS-PM-HL09. URL http://earth.esa.int/ESC2/. ESA.

Melsheimer, C., Tanck, G., Gade, M., & Alpers, W., 1999. Imaging of tidal flats by the SIR-C/X-SAR multi-frequency/multi-polarisation synthetic aperture radar. In Nieuwenhuis, G.J.A., Vaughan, R.A. & Molenaar, M. (Eds). *Operational Remote Sensing for Sustainable Development*. Balkema, Rotterdam, pp. 189-192.

Rainey, M.P., Tyler, A.N., Gilvear, D.J., Bryant, R.G. & McDonald, P., 2003. Mapping intertidal estuarine sediment grain size distributions through airborne remote sensing. *Remote Sensing of Environment*, 86: 480-490.

Salisbury, J.W. & Eastes, J.W., 1985. The effect of particle size and porosity on spectral contrast in the mid-infrared. *Icarus*, 64: 586-588.

Salisbury, J.W. & D'Aria, D., 1992a. Emissivity of terrestrial materials in the 8-14 µm atmospheric window. *Remote Sensing of Environment,* 42: 83-106.

Salisbury, J.W. & D'Aria, D., 1992b. Infrared (8-14µm) remote sensing of soil particle size. *Remote Sensing of Environment,* 42: 157-165.

Smith, G.M., Thomson, A.G., Möller, I., Kromkamp, J.C., 2004. Using hyperspectral imaging for the assessment of mudflat surface stability. *Journal of Coastal Research*, 20: 1165-1175.

Van der Wal, D., Herman, P.M.J. & Wielemaker-van den Dool, 2005. Characterisation of surface roughness and sediment texture of intertidal flats using ERS SAR imagery. *Remote Sensing of Environment,* 98: 96-109.

Van der Wal, D. & P.M.J. Herman, 2006. Regression-based synergy of optical, short-wave infrared and microwave remote sensing for monitoring grain-size of intertidal sediments. *Remote Sensing of Environments* (submitted).

Yates, M.G., Jones, A.R., McGrorty, S., & Goss-Custard, J.D., 1993. The use of satellite imagery to determine the distribution of intertidal surface sediments of the Wash, England. *Estuarine, Coastal and Shelf Science*, 36: 333-344.

ACKNOWLEDGEMENTS

The ERS-2 SAR image used in this study was provided by the European Space Agency (ESA), through project C1P 1426. ASTER data were obtained from ERSDAC and EDC/LPDAAC, and Landsat 7 ETM+ data were obtained from USGS. Support for this study is provided by a grant from the Earth and Life Sciences division of the Netherlands Organisation for Scientific Research, and the Netherlands Institute for Space Research, as part of the User Support Programme for earth observation (ALW/SRON). Jos van Soelen, Bas Koutstaal and Annette Wielemaker-van den Dool assisted in the field and in the laboratory. Peter van Breugel carried out the Malvern analysis. We are grateful to the crew of RV Luctor for logistics.